THE EUROPEAN
PHYSICAL JOURNAL PLUS

An operational approach for accurate ^{177}Lu and ^{177m}Lu activity quantifications to comply with the environmental release criteria: the role of GEANT4 for efficiency curve and True Coincidence Summing effect estimation

Anna Sarnelli[1,a], **Claretta Guidi**[2,b] (iD)**, Luciano Pandola**[3,c] (iD)**, Gian Marco Contessa**[4,d], **Emiliano Loi**[1,e], **David Bianchini**[1,f], **Emilio Mezzenga**[1,g], **Matteo Negrini**[5,h]

[1] Medical Physics Unit, IRCCS Istituto Romagnolo Per Lo Studio Dei Tumori (IRST) "Dino Amadori", 47014 Meldola, Italy
[2] Postgraduate Specialization School in Medical Physics, Alma Mater Studiorum, University of Bologna, 40127 Bologna, Italy
[3] INFN, Laboratori Nazionali del Sud, 95123 Catania, Italy
[4] Italian National Institute of Health, 00161 Rome, Italy
[5] Sezione di Bologna, Istituto Nazionale di Fisica Nucleare, 40126 Bologna, Italy

Abstract The increasing use of ^{177}Lu-labelled agents for targeted radionuclide cancer therapy highlights the radiation protection challenges in the management of radioactive waste due to ^{177m}Lu impurities. To ensure safe disposal, compliance with clearance criteria must be verified using calibrated systems, such as Hyper Pure Germanium (HPGe) spectrometers. This work aims to validate a customized GEANT4 model of our HPGe system in Marinelli beaker geometry to propose an operational approach properly quantifying ^{177}Lu and ^{177m}Lu in waste samples. The system's efficiency curve was calculated by modelling gamma sources in the energy range of interest and validated by spectra measurements of ^{177}Lu and ^{99m}Tc sources. Correction factors accounting for true coincidence summing (TCS) effect were simulated for ^{177}Lu, ^{177m}Lu and ^{99m}Tc and they were applied to the spectrum measurement of a waste sample model with known activities of ^{177}Lu and ^{177m}Lu. Thus, an operational approach for activities quantification was tested comparing the results with the nominal values. No significant differences were observed between simulated and measured efficiency values. TCS correction factors are significant only for ^{177m}Lu (1.6 at 112.95 keV and 204.11 keV). Eventually, the proposed framework to quantify ^{177}Lu in a waste sample allowed to estimate the ^{177}Lu and ^{177m}Lu component activities within a maximum 16% uncertainty. Results show that the HPGe model could be a powerful resource for a wide range of applications in daily clinical routine and it could be used to build a simple quality assurance program to monitor the detector response constancy in time.

1 Introduction

Over the last 2 decades, targeted radionuclide cancer therapy with ^{177}Lu ($T_{1/2} = 6.65$ d [1]) has become of particular interest in the treatment of patients affected by neuroendocrine tumours (NETs) and/or prostate cancers (PCas) due to its intrinsic characteristics. For PCa treatments the main antigen labelled to ^{177}Lu is the prostate-specific membrane antigen (PSMA), while for NET applications common ligand peptides are the somatostatin analogous DOTATATE/DOTATOC [2]. On one hand, the medium-energy beta-particles emission ($E_{max} = 498.3$ keV [1]) with a mean range of 0.7 mm in tissue [3] allows the treatment of small volumes and metastatic lesions with a reduced damage to the healthy tissues. On the other hand, the low-energy gamma emission (the gamma with highest energy emission and highest intensity has about 208 keV [1]) represents a relatively minor concern for radiation protection, while enabling to evaluate the biodistribution in patients with the same radiolabelled preparation used for therapy [4]. The radionuclide can be obtained mainly by nuclear reactors through either a direct method or an indirect process [2, 4]. The direct production path,

[a] e-mail: anna.sarnelli@irst.emr.it (corresponding author)

[b] e-mail: claretta.guidi@studio.unibo.it

[c] e-mail: pandola@lns.infn.it

[d] e-mail: gianmarco.contessa@iss.it

[e] e-mail: emiliano.loi@irst.emr.it

[f] e-mail: david.bianchini@irst.emr.it

[g] e-mail: emilio.mezzenga@irst.emr.it

[h] e-mail: matteo.negrini@bo.infn.it

Springer

consisting in neutron irradiation of a ^{176}Lu target exploiting the ^{176}Lu(n,γ)^{177}Lu reaction, represents the cheapest option to obtain ^{177}Lu. However, it leads to the co-production of ^{177m}Lu, that can often rise some concerns related to radiation protection and waste management due to the longer half-life ($T_{1/2} = 160.4$ d [1]) and the conspicuous gamma emissions compared to ^{177}Lu.

As emphasized by Kurth et al. [5], the success of treatments with DOTATOC/DOTATATE and PSMA ligands may lead to a rise in radionuclide therapies with ^{177}Lu, due to the good outcomes demonstrated in terms of response rates with poor side effects. Having PCa an incidence about 40 times higher than NET in the population and being the second most common cancer in male patients, the interest in ^{177}Lu-PSMA treatments as a clinical practice opportunity is rapidly growing. Hehakaya et al. [6] in 2020 reported that in the Netherlands 4500 patients per year were estimated to be eligible for a 4–6 cycled ^{177}Lu-PSMA treatment.

Patients undergoing treatment with radiopharmaceuticals are carriers of radioactivity, which may be released through sweat, saliva, urine and faeces for a period of time related to the administered radionuclide [7]; this constitutes a radiation protection issue for both hospital personnel and population. Depending on the national legislation, excretions must be collected in an adequate storage system in the hospital facility, following appropriate risk reduction procedures, for a period necessary to comply with the clearance criteria stated by the law for the disposal into the sanitary sewerage system [8, 9]. Following Italian legislation (Decree 101/2020, transposition of the European directive 2013/59/EURATOM), the discharge of radioactive liquid effluents evaluations must be included in the practice authorization procedure with the calculation of specific release formulas for each radionuclide intended to be discharged [10, 11]. This calculation aims to demonstrate the compliance with clearance criteria, ensuring that in all feasible circumstances the cumulative dosimetric impact of all the involved radionuclides on the representative person of the population is less than 10 μSv per year. The same legislation (Art. 67 and Art. 82 of 2013/59/EURATOM, Art. 130 and Art. 151 of Decree 101/2020) imposes the verification of what reported in the authorization prior to each discharge, and stresses the need of regularly calibrate the measuring instruments and check their response stability, with the radiation protection expert being required to verify the instrumentation adequacy (Art. 82, par. 2 in 2013/59/EURATOM and Art. 130, par. 1 in D.Lgs. 101/2020). Therefore, the proper measurement of the radioactivity level and nuclide identification in waste samples are of crucial importance to comply with the clearance criteria, aiming to preserve population and environment from exposures above the limits [12].

To verify liquid waste activity, High Purity Germanium (HPGe) detectors with a Marinelli beaker geometry are commonly used. As semiconductor detectors, they have high efficiency and excellent energy resolution and are widely employed in gamma-spectroscopy and low activity measurements [13]. Even if in Italy there are renowned centres allowing the calibration of these systems, such as the ENEA centre, to the best of our knowledge, this procedure on the whole spectrometric chain using specific geometries related to liquid waste management is rarely available, as well as liquid ^{177}Lu and ^{177m}Lu standardize sources. Therefore, it is common practice that medical physicists, in cooperation with the manufacturer, calibrate and verify the instrumentation following good technical standards, such as BS ISO 20042:2019 [14]. A customized computational model of the whole system could be a fruitful support to set up an appropriate quality assurance program and to calculate the correction factors to be applied in the evaluation of the activity from the measured spectra.

In this view, the first purpose of this work is to validate a Monte Carlo model of the specific Marinelli detection system used in our clinical research institute and to obtain a reference response curve of the system in the energy range of interest. In particular, the work focuses on liquid waste derived from radionuclide therapy with ^{177}Lu. Depending on manufacturer, some ^{177}Lu-based radiopharmaceuticals also present an amount of ^{177m}Lu as impurity. Current Italian legislation allows to exclude radioactive impurities from disposal evaluations, as long as the radiopharmaceuticals involved comply with the applicable good preparation standards (Art. 50, par. 1 in Decree 203/2022). However, since detectable emission peaks of ^{177}Lu are in common with some from the metastable impurity (112.95 keV and 208.37 keV [1]), a correct quantification of ^{177}Lu in the waste sample requires a correct and accurate quantification of ^{177m}Lu. Thus, the secondary aim of this work is to propose a framework to properly quantify the amount of ^{177m}Lu in a waste sample. To the best of our knowledge, the framework here proposed includes for the first time the role of the True Coincidence Summing (TCS) effect on the quantification of ^{177m}Lu. The detection system for Marinelli beaker counting geometry is modelled using GEANT4 (GEometry ANd Tracking) [15].

2 Materials and methods

2.1 Geometry and computational model

The HPGe used in this study is a p-type ORTEC GEM30P4-70 coaxial detector with a Peltier-based cooling system (CFG-X-COOL-III-230) and a nominal resolution of 1.73 keV full width half maximum (FWHM) at 1.33 MeV (second ^{60}Co peak [1]). Its detection volume is composed by a hyper-pure germanium crystal of cylindrical shape with 6.03 cm in height and a nominal diameter of 5.72 cm. According to the manufacturer, the inner dead layer (DL) is made up of a boron-doped layer (P$^+$ contact) with a thickness of 0.30 μm, while the outer DL is a Li-doped layer 0.70 mm thick. An aluminium holder surrounds the sensitive volume, while an external cylindrical aluminium cap encases the whole system. The external cap is located 6.00 cm inside the hole of a cylindrical shield with an external diameter of 45.80 cm and 42.0 cm in height, protecting the detector from the background radiation (e.g. cosmic rays or ^{222}Rn daughters etc.). Such a detector can be used with different geometries, depending on measurement requirements (e.g. blood samples, solid samples etc.).
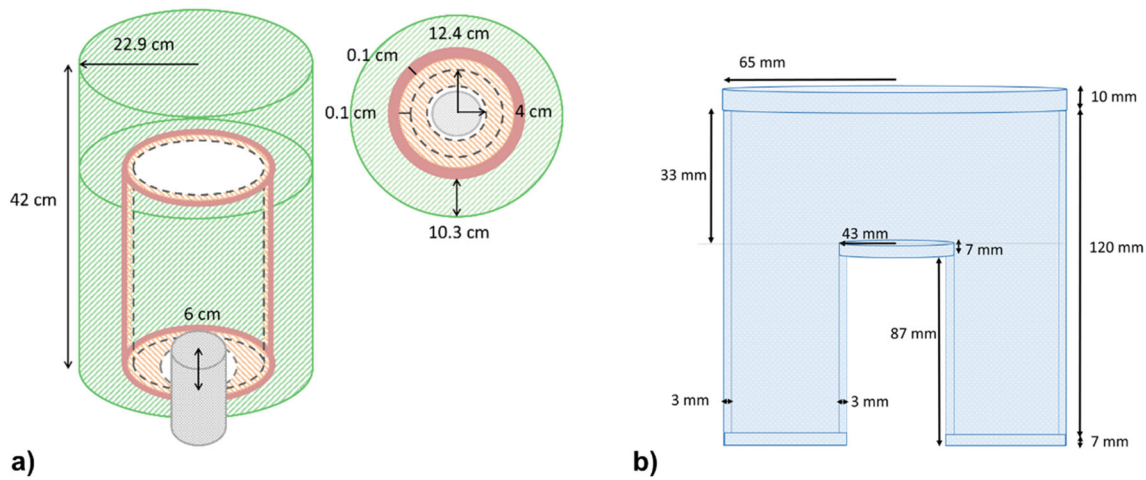
Fig. 1 **a** Scheme and dimensions of the shielding well geometry, with its transversal section in the dashed circle and related dimensions. Colours refer to: lead (green), tin (red) and copper (orange), aluminium (grey). The external aluminium detector cup is 6 cm inside the well cavity. Inside the well, the Marinelli beaker was positioned on the bottom. **b** Transversal section of the one-liter Marinelli beaker model and related dimensions. Blue refers to PMMA
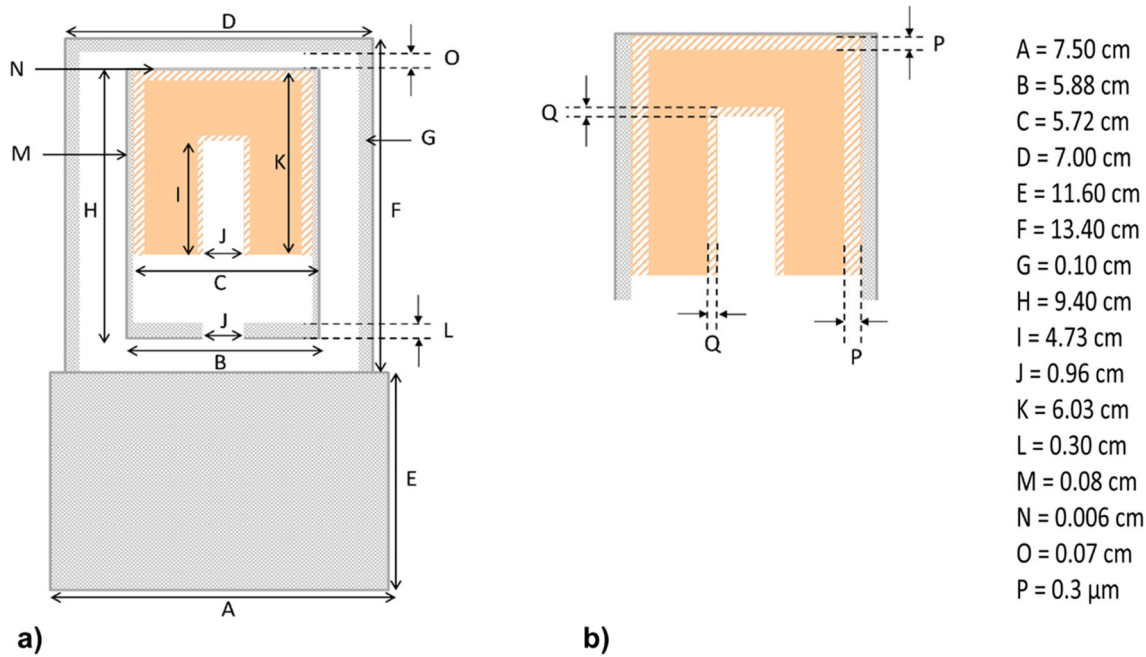

Fig. 2 **a** Simplified scheme of the detector geometry with **b** a zoom on the detector volume and nominal dimensions listed on the right. Colours refer to: germanium (orange), aluminium (grey) and dead layers (streaky orange). The lower part of the aluminium cup of the detector (dimensions A and E) contains electronic components which were not modelled in the simulations

The Marinelli beaker geometry is used to monitor the activity of the excretions over time. The beaker available at our institute is 13.70 cm in height, with an external radius of 6.50 cm and a thickness of 3.00 mm in all lateral walls, entirely made of polymethyl methacrylate (PMMA) and filled with 1 l of water (density = 1.00 g/cm^3). For the measurements, it is always positioned on the bottom of the shielding well, so that the upper wall of the beaker hole is at a height of 2.70 cm from the upper part of the detector aluminium external cap. Representative schemes with detailed dimensions of the cylindrical shield (together with the detector external cap) and the Marinelli beaker are reported in Fig. 1a, b, respectively. The detector model with its detailed dimensions and schemes are shown in Fig. 2.

The whole geometry was simulated with GEANT4 code (version 10.07) [15]. To replicate the detector response, both internal and external DLs were implemented with the nominal dimensions listed in Fig. 2. According to other authors [16, 17], DLs were approximated as partial volumes of the germanium crystal in which no energy deposition contributes to the total energy record. The detector active volume was set as the scoring volume, where the total energy deposited per event was scored. To allow appropriate

Table 1 Calibration parameters used in Eqs. 1 and 2

	a	b	c	d	e	f
Value	0.26	0.25	1.09×10^{-8}	3.22	9.82×10^{-4}	5.15×10^{-8}

Parameter c and f are negligible

Fig. 3 Simplified decay scheme of ^{177m}Lu and ^{177}Lu. All energies are expressed in keV. Photon data were compiled from Nucléide Lara database [1], some electron and energy level data were taken from National Nuclear Database Center [19]
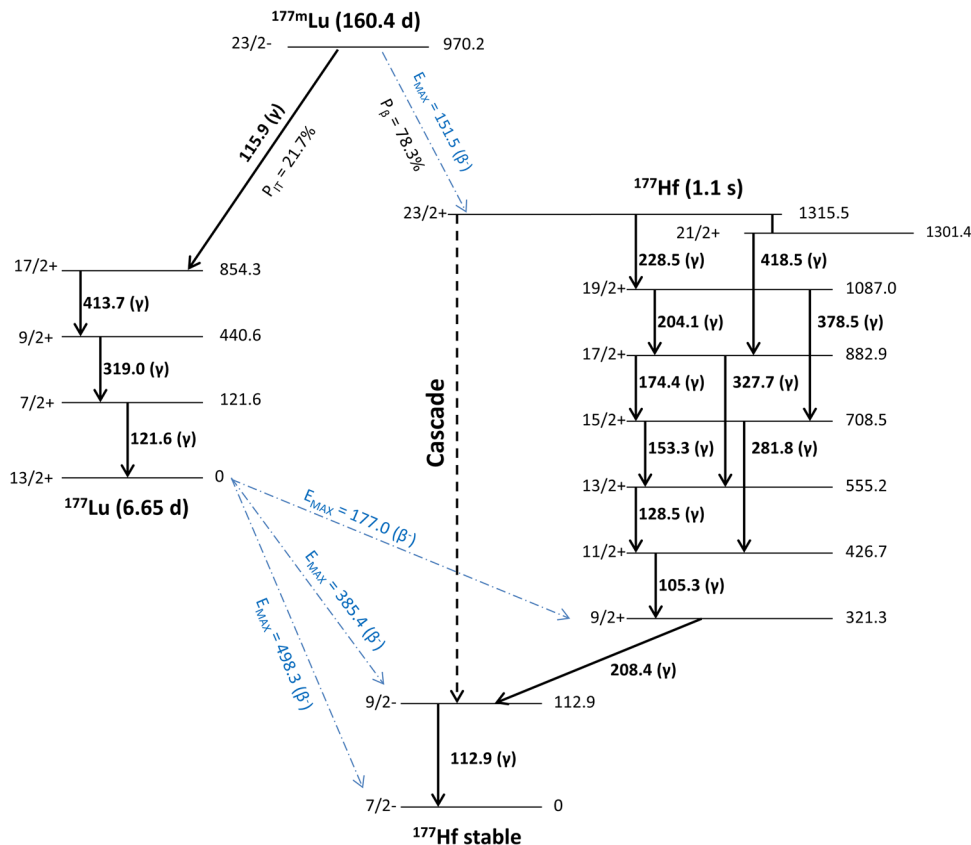
comparison between simulated and measured data, the system resolution was implemented [18] combining the FWHM and energy calibrations as:

$$\text{FWHM}(C) = a + b \cdot C + c \cdot C^2 \tag{1}$$

$$E = d + e \cdot C + f \cdot C^2 \tag{2}$$

where a, b, c, d, e, f are parameters extracted from instrument calibrations (Table 1) and C is the channel of the multichannel analyser, corresponding to a certain energy E. Thus, an expression of the FWHM as a function of energy, FWHM(E), was obtained, representing our specific HPGe system resolution characteristics. Quadratic terms are negligible (Table 1). A gaussian smearing was applied to each simulated deposit of energy E_0 in the scoring volume, with mean E_0 and standard deviation σ_{E_0} given by [18]:

$$\sigma_{E_0} = \frac{\text{FWHM}(E_0)}{\sqrt{8 \cdot \ln(2)}} \tag{3}$$

2.2 Sources

Three different radionuclides are considered for this study: ^{99m}Tc, pure ^{177}Lu and combined ^{177}Lu–^{177m}Lu. The ^{99m}Tc decay ($T_{1/2}$ = 6.01 h) has two possible branches [1]. Since the gamma emissions derived from the ^{99m}Tc β^- branch and from the ^{99}Tc decay have intensities well below 1%, they can be neglected and the only relevant one is that at 140.51 keV derived from the ^{99m}Tc Isomeric Transition (IT) branch, with an absolute intensity of 88.5% (Table 2).

^{177m}Lu decay ($T_{1/2}$ = 160.4 d) has two distinct branches, as schematized in Fig. 3 [1, 19]: in the 78.3% of cases, it decays β^- into ^{177}Hf stable, whereas in 21.7% it undergoes IT to ^{177}Lu ($T_{1/2}$ = 6.65 d), which in turn decays 100% β^- into ^{177}Hf stable. The main gamma emissions due to ^{177m}Lu and ^{177}Lu decays are listed in Table 2 with corresponding intensities in percentage.

Table 2 Summary of the main ^{177m}Lu, ^{177}Lu and ^{99m}Tc emissions

^{177}Lu → ^{177}Hf 100% β⁻ decay			
GAMMAS		**ELECTRONS**	
Energy (keV)	Intensity (%)	End-point energy (keV)	Intensity (%)
112.9498 *4*	6.20 *7*	177.0 *8*	11.64 *10*
208.3662 *4*	10.38 *7*	385.4 *8*	9.1 *5*
		498.3 *8*	79.3 *5*

^{177m}Lu → ^{177}Hf

^{177m}Lu → ^{177}Hf (78.3% β⁻ decay)		^{177m}Lu → ^{177}Lu (21.70% Isomeric Transition (IT))	
GAMMAS		**GAMMAS**	
Energy (keV)	Intensity (%)	Energy (keV)	Intensity (%)
105.3595 *6*	12.3 *3*	319.0205 *8*	10.5 *5*
112.9498 *5*	20.4 *5*	413.6636 *7*	17.4 *8*
128.503 *5*	15.5 *4*		
153.2843 *5*	16.9 *4*		
204.1052 *5*	13.8 *4*		
208.3662 *4*	57.7 *12*		
228.4838 *6*	37.0 *8*		
281.7873 *9*	14.1 *4*		
327.6829 *7*	18.1 *5*		
378.5029 *7*	29.7 *13*		
418.5391 *7*	21.3 *9*		

ELECTRONS		**ELECTRONS**	
End-point energy (keV)	Intensity (%)		
151.5 *8*	78.30 *8*		
Others: conversion electrons		Only conversion electrons	

^{99m}Tc → ^{99}Tc 99.996% IT	
GAMMAS	
Energy (keV)	Intensity (%)
140.511 *1*	88.5 *2*

Photon data were taken from Nucléide Lara database [1], some electron data were taken also from National Nuclear Database Center [19]. Intensities are absolute intensities, i.e. emission probability per decay. The ^{177m}Lu peak at (174.3991 ± 0.0005) keV was excluded from the list, although with an emission intensity of (12.6 ± 0.3) %, because part of a triplet region of the spectrum. Uncertainties are reported in italics and they are meant on the last digit
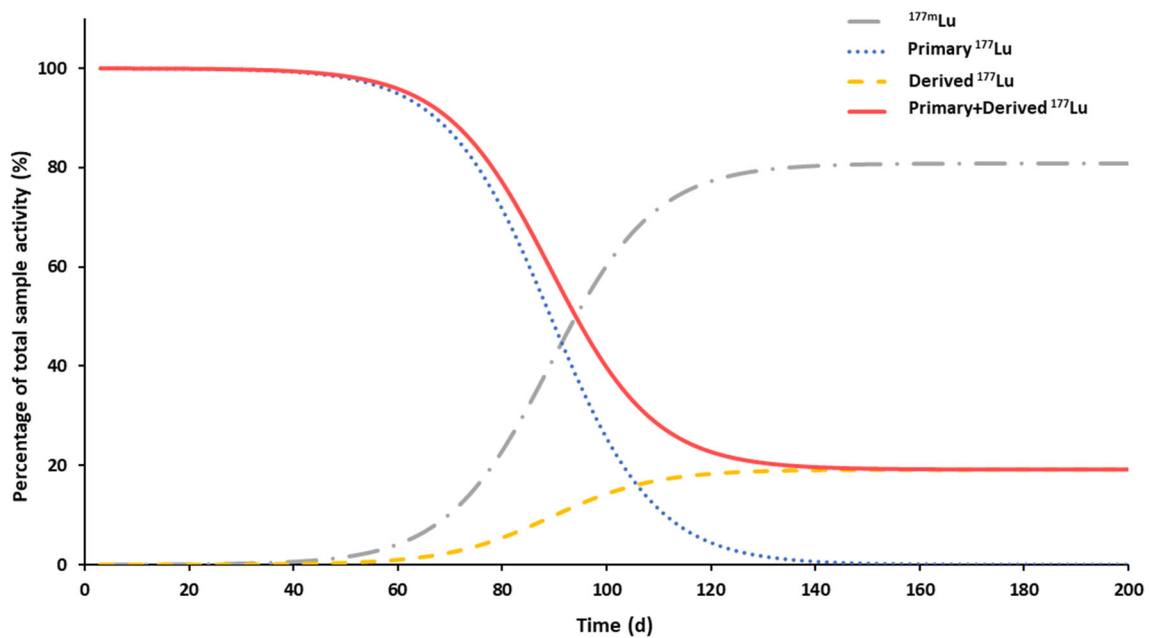
Fig. 4 Percentage contributions to the total activity of the combined ^{177}Lu–^{177m}Lu source sample. The red solid line represents the whole ^{177}Lu activity contribution, as a sum of the primary and derived components

A ^{177}Lu direct-produced liquid source, uniformly distributed in 1 l of water, was exploited as a combined ^{177}Lu–^{177m}Lu source, mimicking a radioactive waste sample to be disposed in the sanitary sewerage system, with both activity components certified. The total activity of the sample is a consequence of the emissions from primary ^{177}Lu, ^{177m}Lu-derived ^{177}Lu and ^{177m}Lu impurities. Despite the limited amount, ^{177m}Lu has a half-life about 24 times longer than that of ^{177}Lu, thus transient equilibrium [20] is achieved between ^{177}Lu and ^{177m}Lu-derived ^{177}Lu [21]. Thus, long after production, the amount of ^{177}Lu drastically decreases and almost all the activity is attributable to the decay of ^{177m}Lu. In Fig. 4 the percentage contribution of primary ^{177}Lu, ^{177m}Lu-derived ^{177}Lu and ^{177m}Lu to the total activity of a ^{177}Lu direct-produced liquid source is represented. As can be observed, initially the sample activity is all attributable to the primary ^{177}Lu, being the main sample component, while ^{177m}Lu component is roughly negligible. Over time, the derived ^{177}Lu contribution increases thanks to ^{177m}Lu decay. However, ^{177}Lu activity decreasing in time is drastically faster than the ^{177m}Lu one, due to its characteristic half-life. Being the total sample activity given by the sum of all component activities, it follows that after a certain period of time ^{177m}Lu contribution will dominate on ^{177}Lu.

2.3 Single energy full-energy peak efficiency curve: simulation and validation

To obtain a reference full-energy peak (FEP) efficiency curve of the detection system in the energy range of interest, a source of isotropic and monochromatic photons was implemented inside the model of the Marinelli beaker, uniformly distributed in the water. The efficiency curve obtained this way was labelled as "Single Energy" or SE and represented the ideal efficiency curve of the acquisition system in the chosen geometry and sample type. Runs were performed each time simulating 10^6 events and selecting one of the main gamma peaks of ^{177}Lu, ^{177m}Lu and ^{99m}Tc decays listed in Table 2 as source energy. Each point of the curve $\left(\text{FEP}_E^{SE}\right)$ was calculated as the ratio between the net area under the peak at the selected energy (NA_E) and the number of photons simulated during the correspondent run:

$$\text{FEP}_E^{SE} = \frac{\text{NA}_E}{10^6} \tag{4}$$

NA calculations were based on the summing method [14, 22] and the energy integration interval was always considered as ± 1.5 FWHM centred in the maximum of the selected peak, whose energy dependence was extrapolated from Eq. 1 and Eq. 2.

To validate the FEP^{SE} curve and the HPGe model, comparisons with measurements in the same conditions were needed [14]. Since ^{177m}Lu has a complex decay scheme with many cascade gamma emissions, the ^{99m}Tc and the pure ^{177}Lu sources were chosen for the purpose. Known activities were uniformly distributed in the Marinelli beaker described in Sect. 2.1 and the same setup was adopted to acquire spectra with dead time always lower than 2%. Each measured FEP efficiency point, FEP$_E^{meas}$, was obtained as:

$$\text{FEP}_E^{meas} = \frac{\text{NA}_E^i}{A_i(t_0) \cdot \Delta t \cdot I_E^i} \tag{5}$$

where $A_i(t_0)$ is the nominal activity of the source containing the radionuclide i (i.e. ^{99m}Tc or ^{177}Lu) at the measurement time t_0 and I_E^i is the gamma emission intensity at the energy E of the radionuclide i (Table 2). $A_i(t_0)$ was considered constant during the measurements because of the short live time ($\Delta t = 3600$ s) with respect to the nuclide half-lives considered. As the ^{99m}Tc was the radionuclide with the shortest half-life (6 h), NA$_{140.51}$ could have been the most affected by the activity decreasing during measurements. Accounting for this effect, a percentage difference of about 5.6% in the FEP value at 140.51 keV was derived, which was comparable with the measure relative error (approximately 6.6%). Hence, the assumption of constant $A_i(t_0)$ was maintained during all efficiency calculations.

2.4 True Coincidence Summing effect: simulation and validation

TCS effect is a well-known phenomenon [22–27] that alters the photopeak counts at different energies: two or more photons emitted within a shorter time than the detector response time can be detected as a single photon event, with an energy given by the sum of each deposition. As the effect is activity-independent [23], the HPGe model was exploited to obtain TCS correction factors for each gamma emission energy of ^{177m}Lu, ^{177}Lu and ^{99m}Tc decays [28]. For this purpose, simulations were performed both removing (referred as "Partial Decay", or PD) and including (referred as "Total Decay", or TD) the TCS effect. Both simulations included the same number of source nuclei of the selected radionuclides (^{177m}Lu, ^{177}Lu or ^{99m}Tc), uniformly distributed at rest in the Marinelli beaker water, and the use of the GEANT4 decay simulation package [29]. To perform PD simulations, all the gamma tracks resulting from the source decays were suppressed immediately when generated, except those at a specified energy: This was performed each run varying the energy value until the gamma energies listed in Table 2 were all considered. On the contrary, to perform TD simulations all the decay-derived tracks were included: In this way, all the photons belonging to the same cascade and releasing energy in the detector active volume were treated as a single event with energy given by the sum of the gamma energies released throughout the cascade.

For both PD and TD simulations, spectra were registered and each NA under the photopeak at a certain energy E (NA^{PD} and NA^{TD}, respectively) was calculated. From the ratio between NA^{PD} and NA^{TD} at the same energy E, simulated TCS correction factors (TCS^{sim}) were calculated for each gamma emission energy of interest:

$$\text{TCS}^{\text{sim}} = \frac{\text{NA}^{\text{PD}}}{\text{NA}^{\text{TD}}} \tag{6}$$

The simulated factors were compared with the experimental ones (TCS^{exp}) calculated on independent measures as:

$$\text{TCS}^{\text{exp}} = \frac{\text{EC}}{\text{NA}_{\text{meas}}} \tag{7}$$

where NA$_{meas}$ is the net area measured under the photopeak at energy E, and the expected counts (EC) at the same energy were calculated as:

$$\text{EC} = \Delta t \cdot \text{FEP}^{\text{SE}} \cdot \left(A_{\text{mLu}}(t_0) \cdot I^{\text{mLu}} + A_{\text{Lu}}(t_0) \cdot I^{\text{Lu}} \right) \tag{8}$$

where I^{mLu} and I^{Lu} are the gamma emission intensities at energy E of ^{177m}Lu and ^{177}Lu, respectively. For non-in-common photopeaks, I^{Lu} was considered equal to 0.

2.5 Lutetium quantification

To test the previously calculated FEP^{SE} curve in the high energy range, a direct-produced ^{177}Lu source was exploited as a combined ^{177m}Lu–^{177}Lu source mimicking an ideal radioactive waste sample, with both activity contributions certified. The FEP^{SE} curve was adopted for quantifying the contribution of the ^{177m}Lu component to the total activity. The ^{177m}Lu–^{177}Lu source spectrum was acquired in the same setup described in Sect. 2.1. To quantify the amount of ^{177m}Lu in the source, the NAs at the characteristic ^{177m}Lu gamma emission energies not in common with the ^{177}Lu ones were calculated (NA$_E^{\text{mLu}}$) and corrected by the corresponding TCS^{sim} factors (Eq. 6). Using the FEP^{SE} efficiency curve previously obtained, the activity of ^{177m}Lu in the sample was estimated as the weighted mean of the activity calculated on each photopeak of interest:

$$A_{\text{mLu}}(t_0, E) = \frac{\text{TCS}_E^{\text{sim}} \cdot \text{NA}_E^{\text{mLu}}}{\text{FEP}_E^{\text{SE}} \cdot \Delta t \cdot I_E^{\text{mLu}}}$$

$$A_{\text{mLu}}(t_0) = \frac{\sum_E A_{\text{mLu}}(t_0, E)/\delta_E^2}{\sum_E 1/\delta_E^2} \tag{9}$$

where $A_{\text{mLu}}(t_0, E) = {}^{177m}$Lu activity estimated from photopeak at energy E and δ_E^2 is the square of the associated uncertainty. $A_{\text{mLu}}(t_0)$ was used to calculate the number of counts that contribute to the area of the photopeaks at 112.95 keV and 208.37 keV due to the ^{177m}Lu decay only (i.e. C_E^{mLu} in Eq. 8). Then, by subtraction, it was possible to calculate the counts under the area of the

Fig. 5 Efficiency curve versus energy related to single energy (SE) simulations and measurements of ^{177}Lu and ^{99m}Tc sources
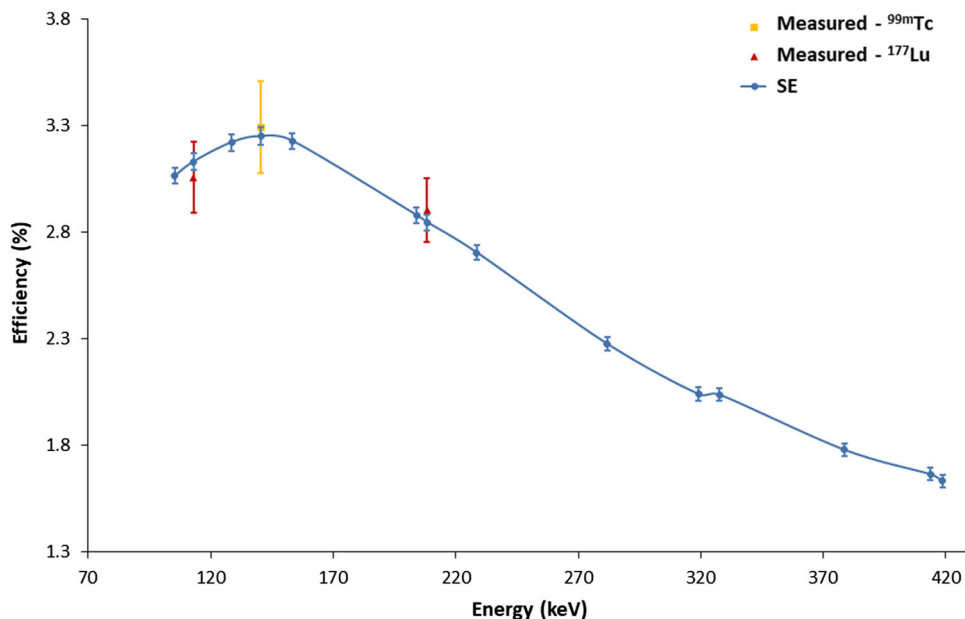

Table 3 FEP^{SE} efficiency values and calculated values from measured spectra of pure ^{177}Lu and ^{99m}Tc sources

Energy	Simulated	Measured		Diff (%)
	SE Eff (%)	^{177}Lu Eff (%)	^{99m}Tc Eff (%)	
105.36	3.06 ± 0.04			
112.95	3.13 ± 0.04	3.1 ± 0.2		1
128.50	3.22 ± 0.04			
140.51	3.25 ± 0.04		3.3 ± 0.2	-2
153.28	3.23 ± 0.04			
204.10	2.88 ± 0.04			
208.37	2.84 ± 0.04	2.9 ± 0.2		-1
228.48	2.70 ± 0.03			
281.79	2.27 ± 0.03			
319.02	2.04 ± 0.03			
327.68	2.04 ± 0.03			
378.50	1.78 ± 0.03			
413.67	1.66 ± 0.03			
418.54	1.63 ± 0.03			

In the last column percentage relative differences between simulated and measured values are reported

photopeaks at 112.95 keV and 208.37 keV due to the ^{177}Lu decay only (NA$_E^{Lu}$, Eq. 10), and to calculate the activity of the ^{177}Lu component in the sample ($A_{Lu}(t_0)$) using Eq. 9 adapted to ^{177}Lu quantities and emission energies:

$$\text{NA}_E^{Lu} = \text{NA}_E^{Lu + mLu} - C_E^{mLu} = \text{NA}_E^{Lu + mLu} - \left(A_{mLu}(t_0) \cdot \text{FEP}_E^{SE} \cdot \Delta t \cdot I_E^{mLu} \right) \tag{10}$$

where NA$_E^{Lu + mLu}$ is the net area measured at energy E on the whole source spectrum.

3 Results

The FEP^{SE} efficiency curve was validated in the low energy range by the measurements of the pure ^{177}Lu and ^{99m}Tc sources (Fig. 5), with a maximum absolute relative difference of 2% between the simulated SE efficiency value (2.84%) and the measured value (2.9%) deriving from the ^{177}Lu spectrum acquisition (Table 3). This difference was observed at 208.37 keV and turned out to be comparable with the ^{177}Lu-derived maximum relative uncertainty (about 7%).

Fig. 6 Comparison between the
measured and the simulated TD
spectra of the radionuclide
sources: **a** ^{177}Lu–^{177m}Lu,
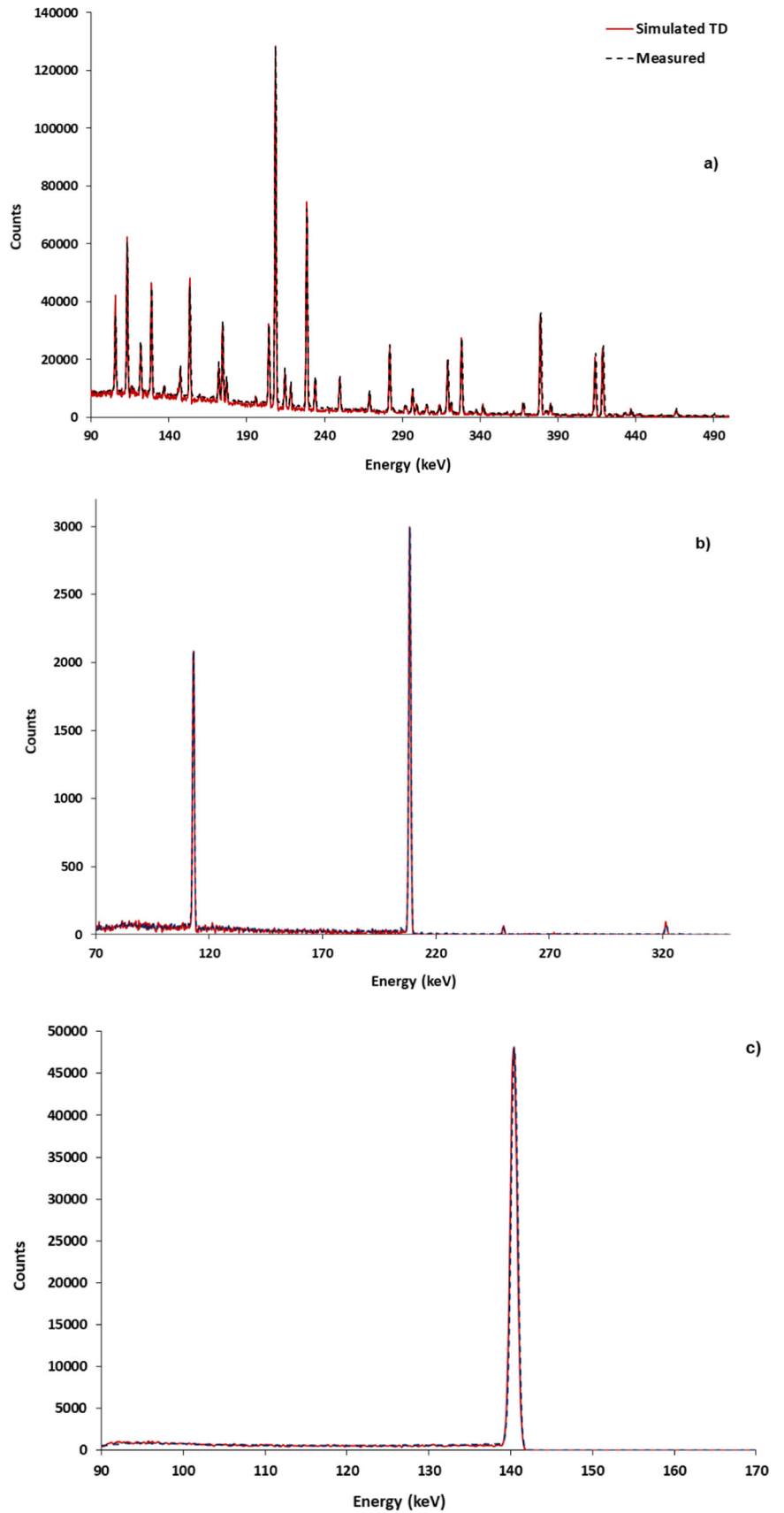**b** ^{177}Lu, **c** ^{99m}Tc

Fig. 7 Comparison between the partial decay (PD) and the total decay (TD) simulated spectra of the radionuclide sources: **a** ^{177m}Lu, **b** ^{177}Lu, **c** ^{99m}Tc. Not all the gamma emission energies of the ^{177m}Lu decay were considered in the PD simulations
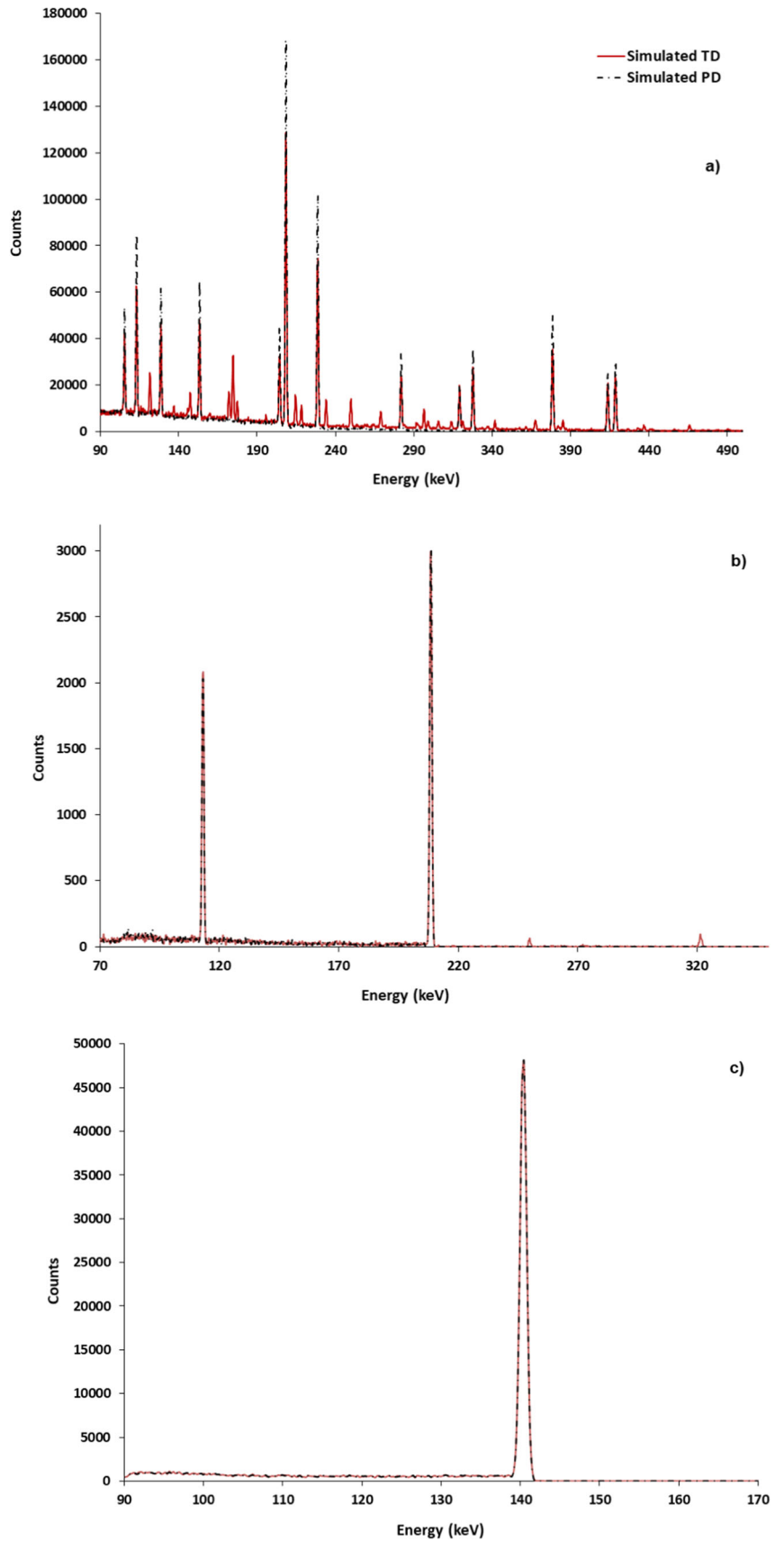
Table 4 Simulated and measured TCS correction factors at different energies for ^{177m}Lu, ^{177}Lu and ^{99m}Tc sources

Energy (MeV)	^{177m}Lu		^{177}Lu		^{99m}Tc	
	TCS^{sim}	TCS^{exp}	TCS^{sim}	TCS^{exp}	TCS^{sim}	TCS^{exp}
105.36	1.4±0.1	1.5±0.2				
112.95	1.6±0.1		1.00±0.08	1.02±0.05		
128.50	1.5±0.1	1.4±0.2				
140.51					1.00±0.06	1.03±0.01
153.28	1.38±0.09	1.5±0.2				
204.11	1.6±0.1	1.5±0.2				
208.37	1.41±0.04		1.04±0.06	0.98±0.05		
228.48	1.40±0.05	1.4±0.2				
281.79	1.5±0.1	1.4±0.2				
319.02	1.2±0.1	1.1±0.1				
327.68	1.4±0.1	1.3±0.2				
378.50	1.40±0.07	1.3±0.1				
413.66	1.4±0.1	1.2±0.1				
418.54	1.5±0.1	1.2±0.2				

TCS^{exp} related to common ^{177m}Lu and ^{177}Lu peaks were not calculated due to the absence of information on counts under these peaks certainly attributable to ^{177m}Lu

Table 5 Activities of the ^{177}Lu and ^{177m}Lu components of the therapy-derived radioactive liquid waste sample emulator, nominal (second column) and derived from the spectrum analysis (third column)

Radionuclide	Activity (kBq)		Discrepancy (%)
	Nominal	Derived	
^{177}Lu	8±1	10±2	16
^{177m}Lu	25±3	25.4±0.2	3

Discrepancies are not significant, as TCS correction factors were applied to the NAs

Figure 6a shows the measured ^{177m}Lu–^{177}Lu, pure ^{177}Lu (Fig. 6b) and ^{99m}Tc (Fig. 6c) spectra, exhibiting a good agreement with the TD-simulated ones, rescaled by proper scaling factors. TD-simulated spectra were compared with PD-simulated ones (Fig. 7), that were obtained by summing the corresponding mono-peak PD spectra. The ^{177m}Lu spectra showed an appreciable disagreement due to the TCS effect, as well as the absence of some photopeaks not considered in this work due to the low associated emission intensities or the presence of multiplet regions (Fig. 7a). Conversely the ^{177}Lu and the ^{99m}Tc PD-simulated spectra were comparable with the corresponding TD-simulated ones (Fig. 7b, c).

The TCS correction factors, calculated for each source from PD and TD simulations, are listed in Table 4. While for ^{177}Lu and ^{99m}Tc values approached unity for each gamma emission energy, correction factors associated to the ^{177m}Lu source were more significant and varied at different emission energies. The simulated TCS factors were comparable with the measured ones in the selected energy range (Table 4). A maximum absolute relative difference of 7% (at 327.68 keV) was observed in the energy range from 105.36 to 378.50 keV. At 413.66 keV and 418.54 keV absolute relative differences of about 18% were observed, however values were comparable with simulated ones.

Eventually, Table 5 shows the estimated activities of the ^{177}Lu and ^{177m}Lu components of the composited source. Discrepancies of maximum 16% could be noted, not significantly different from the nominal values.

4 Discussion and conclusion

In this work, the customized GEANT4 model of the HPGe detection system available at our institute was implemented with a Marinelli beaker geometry. Using this model, the FEP efficiency calibration curve of the system in the working energy range (from about 100 keV to about 420 keV [1]) was calculated by SE simulations, as described in Sect. 2.3. This curve should offer the most accurate evaluation of the system efficiency achievable, being unaffected by the complex mechanisms originating from source decays and depending only on the acquisition geometry (including the sample type) and the detected gamma energies. FEP efficiency values calculated from the acquisition of the pure ^{177}Lu and ^{99m}Tc sources spectra validated the FEP^{SE} curve in the low energy range.

To test the higher energy range of the curve, a different approach was adopted, which allowed both to exploit the potential of the computational model and to propose an operational framework for quantifying the ^{177m}Lu component in a therapy-derived liquid waste sample. The dosimetric impact of ^{177m}Lu is at least an order of magnitude greater than that of ^{177}Lu, as shown by the

weight factors given in the NCRP Report No.123 to calculate the release formulas [10]. Therefore, from an ethical and a radiation protection point of view, its careful evaluation contributes to compliance with the ALARA principle and ensures a correct evaluation of the before mentioned release formula. Thus, a therapy-derived liquid waste sample was simulated by a direct-produced ^{177}Lu source containing ^{177m}Lu as impurity, with both activity contributions certified. The NAs of the ^{177m}Lu characteristic photopeaks were calculated to estimate the ^{177m}Lu activity component in the sample, considering the FEP^{SE} curve valid for this measure setup. However, due to the complexity of the ^{177m}Lu decay scheme, a strong TCS effect was expected during the spectrum measurement. The HPGe GEANT4 model was adopted to simulate partially (PD) or completely (TD) influenced spectra from whom to estimate the TCS correction factors for ^{177}Lu, ^{177m}Lu and ^{99m}Tc sources. The positive outcome of the comparison between the measured and the TD-simulated spectra (properly rescaled) ensured an accurate reproduction of the radioactive decay processes of ^{177}Lu, ^{177m}Lu and ^{99m}Tc sources by the GEANT4 decay simulation package. Minimal variations may have been caused by small inaccuracies in the GEANT4 library of gamma emission intensities. Moreover, the accuracy given by the manufacturer in geometrical specifications could also have been very relevant: Other works show that discrepancies in the real distances, dead layers and material thicknesses compared to the nominal values could lead to even significant variations [16, 17].

Confirming the expectation, significant discrepancies were noted comparing the PD and TD ^{177m}Lu simulated spectra, whereas the similar comparisons for ^{177}Lu and ^{99m}Tc sources showed good agreements. This was because the simpler, cascade-poorer decay schemes of ^{177}Lu and ^{99m}Tc compared to ^{177m}Lu, hence showing a negligible TCS effect. Confirmation was found in TCS correction factors obtained for each energy and radionuclide of interest: for both ^{177}Lu and ^{99m}Tc spectra they were unitary at all gamma emission energies, whereas for ^{177m}Lu spectrum the lowest value of 1.2 was obtained at 309.02 keV. Thus, TCS^{sim} factors were applied to correct the net areas of the photopeaks related to the ^{177m}Lu decay only, calculated on the acquired spectra of the combined ^{177m}Lu–^{177}Lu source mimicking the radioactive waste sample. The estimation of the ^{177m}Lu activity component in the sample was adopted to derive the ^{177}Lu activity contribution.

As TCS effect does not affect ^{177}Lu spectrum acquisition, it worth noting that during ^{177m}Lu and ^{177}Lu quantification TCS^{sim} factors related to the common photopeaks should be applied to the portion of counts associated with the ^{177m}Lu decay only. Being these TCS^{sim} factors greater than 1 for all emission energies, their application to the whole peaks could lead to an overestimation of the ^{177}Lu activity in the sample. This overestimation is certainly conservative from the perspective of clearance, but it may impact in the clinical flow management and storage system sizing optimization. However, if measurements are performed at a time point ensuring a strong predominance of ^{177m}Lu contribution to the total sample activity, ^{177}Lu overestimation pitfalls could be reasonably acceptable in favour of a streamlined and timesaving procedure. Results showed good agreements with the nominal values for both the radionuclide components, thus completing the validation of the HPGe computational model, the FEP^{SE} curve and the TCS^{sim} correction factors.

Once validated, the HPGe model could be exploited for a wide range of applications such as planning a robust quality assurance program, investigating the causes of possible drifts in system stability or extend and verify the system response with other geometries or complex radionuclides of interest adopted in daily clinical routine (e.g. ^{131}I). Moreover, it could be adopted to obtain different crucial correction factors (e.g. density correction, self-absorption correction, etc.) in other context [30–32], for example in the field of radiopharmaceutical purity controls.

In conclusion, the potential and the versatility of the Monte Carlo approach make this model a powerful resource for a wide range of applications, not only in a research facility but also in a daily clinical routine. Regarding the discharge of radioactive effluents, it could be a useful tool to ensure an effective application of the optimization of the radiation protection of members of the public, according to the provisions of the directive 2013/59/EURATOM [33].

Data Availability Statement This manuscript has associated data in a data repository. [Authors' comment: Spectra generated and analysed during the current study are available from the corresponding author on reasonable request. For data request, please contact anna.sarnelli@irst.emr.it].

Declarations

Conflict of interest Authors declare that they have no known competing financial or non-financial interests to declare that are relevant to the content of this work.

References

1. Library for gamma and alpha emissions, Nucléide Lara. http://www.lnhb.fr/Laraweb. Accessed 03 Dec 2023.
2. R. Chakravarty, S. Chakraborty, Am. J. Nucl. Med. Mol. Imaging **11**, 443 (2021)
3. H. Ahmadzadehfar, K. Rahbar, M. Essler, H.J. Biersack, Semin. Nucl. Med. (2020). https://doi.org/10.1053/j.semnuclmed.2019.07.003
4. A. Dash, M.R.A. Pillai, F.F. Knapp, Nucl. Med. Mol. Imaging (2015). https://doi.org/10.1007/s13139-014-0315-z
5. J. Kurth, B.J. Krause, S.M. Schwarzenböck, L. Stegger, M. Schäfers, K. Rahbar, EJNMMI Res. (2018). https://doi.org/10.1186/s13550-018-0386-4
6. C. Hehakaya, E.H.M. Moors, H.M. Verkooijen, D.E. Grobbee, F.A. Verburg, M.G.E.H. Lam, Eur. J. Nucl. Med. Mol. Imaging (2021). https://doi.org/10.1007/s00259-020-05102-4
7. J.J. Cuaron, A.E. Hirsch, D.C. Medich, J.A. Hirsch, B.S. Rosenstein, J. Am. Coll. Radiol. (2011). https://doi.org/10.1016/j.jacr.2010.08.020
8. R. Ravichandran, J. Binukumar, R. Sreeram, L. Arunkumar, J. Med. Phys. (2011). https://doi.org/10.4103/0971-6203.79692
9. K.L. Nelson, M.A. Sheetz, Health Phys. (2019). https://doi.org/10.1097/HP.0000000000001122
10. National Council on Radiation Protection and Measurement, *NCRP Report 123: Screening Models for Releases of Radionuclides to Atmosphere, Surface Water, and Ground* (NCRP, Bethesda, 1996)
11. G.M. Contessa, M. D'Arienzo, M. Frisoni, P. Ferrari, R. Panichi, F. Moro, A. Pietropaolo, Eur. Phys. J. Plus (2021). https://doi.org/10.1140/epjp/s13360-021-01404-0
12. United States Environmental Protection Agency, *Federal Guidance Report No. 15: External Exposure to Radionuclides in Air, Water and Soil* (EPA, Oak Ridge, 2019)
13. G.F. Knoll, *Radiation Detection and Measurement*, 3rd edn. (Wiley, 2000)
14. British Standard and International Organization for Standardization, *BS ISO 20042:2019: Measurement of Radioactivity-Gamma-Ray Emitting Radionuclides-Generic Test Method Using Gamma-Ray Spectrometry*, 1st edn. (BSI Standards Limited, 2019).
15. S. Agostinelli, J. Allison, K. Amako, J. Apostolakis, H. Araujo, P. Arce, M. Asai, D. Axen, S. Banerjee, G. Barrand, F. Behner, L. Bellagamba, J. Boudreau, L. Broglia, A. Brunengo, H. Burkhardt, S. Chauvie, J. Chuma, R. Chytracek, G. Cooperman, G. Cosmo, P. Degtyarenko, A. Dell'Acqua, G. Depaola, D. Dietrich, R. Enami, A. Feliciello, C. Ferguson, H. Fesefeldt, G. Folger, F. Foppiano, A. Forti, S. Garelli, S. Giani, R. Giannitrapani, D. Gibin, J. J. Gómez Cadenas, I. González, G. Gracia Abril, G. Greeniaus, W. Greiner, V. Grichine, A. Grossheim, S. Guatelli, P. Gumplinger, R. Hamatsu, K. Hashimoto, H. Hasui, A. Heikkinen, A. Howard, V. Ivanchenko, A. Johnson, F. W. Jones, J. Kallenbach, N. Kanaya, M. Kawabata, Y. Kawabata, M. Kawaguti, S. Kelner, P. Kent, A. Kimura, T. Kodama, R. Kokoulin, M. Kossov, H. Kurashige, E. Lamanna, T. Lampén, V. Lara, V. Lefebure, F. Lei, M. Liendl, W. Lockman, F. Longo, S. Magni, M. Maire, E. Medernach, K. Minamimoto, P. Mora de Freitas, Y. Morita, K. Murakami, M. Nagamatu, R. Nartallo, P. Nieminen, T. Nishimura, K. Ohtsubo, M. Okamura, S. O'Neale, Y. Oohata, K. Paech, J. Perl, A. Pfeiffer, M. G. Pia, F. Ranjard, A. Rybin, S. Sadilov, E. di Salvo, G. Santin, T. Sasaki, N. Savvas, Y. Sawada, S. Scherer, S. Sei, V. Sirotenko, D. Smith, N. Starkov, H. Stoecker, J. Sulkimo, M. Takahata, S. Tanaka, E. Tcherniaev, E. Safai Tehrani, M. Tropeano, P. Truscott, H. Uno, L. Urban, P. Urban, M. Verderi, A. Walkden, W. Wander, H. Weber, J. P. Wellisch, T. Wenaus, D. C. Williams, D. Wright, T. Yamada, H. Yoshida, D. Zschiesche, Nucl. Instrum. Methods Phys. Res. (2003). https://doi.org/10.1016/S0168-9002(03)01368-8.
16. G. J. De, S. Corrêa, W. F. Rebello, R. K. Morales, D. O. Cardoso, S. C. A. Corrêa, A. X. Da Silva, in *2011 International Nuclear Atlantic Conference - INAC 2011* (ABEN, Belo Horizonte, 2011)
17. F. Courtine, T. Pilleyre, S. Sanzelle, D. Miallier, Nucl. Instrum. Methods Phys. Res. A (2008). https://doi.org/10.1016/j.nima.2008.07.155
18. G. Gilmore, *Practical Gamma-Ray Spectrometry*, 2nd edn. (Wiley, Warrington, 2008)
19. National Nuclear Data Center Website, NuDat 3.0, https://Www.Nndc.Bnl.Gov/Nudat3. Accessed 06 April 2023.
20. J.T. Bushberg, A.J. Seibert, E.M. Leidholdt, J.M. Boone, *The Essential Physics of Medical Imaging*, 3rd edn. (Lippincott Williams & Wilkins, Philadelphia, 2012)
21. D. Kupitz, E. Einspänner, H. Wissel, A. Hohn, M.C. Kreissl, O.S. Grosser, Med. Phys. (2022). https://doi.org/10.1002/mp.15951
22. M.C. Lépy, A. Pearce, O. Sima, Metrologia (2015). https://doi.org/10.1088/0026-1394/52/3/S123
23. E. Tomarchio, S. Rizzo, Radiat. Phys. Chem. (2011). https://doi.org/10.1016/j.radphyschem.2010.09.014
24. A.M. Ababneh, M.M. Eyadeh, J. Radiat. Res. Appl. Sci. (2015). https://doi.org/10.1016/j.jrras.2015.05.003
25. J.-M. Laborie, G. le Petit, D. Abt, M. Girard, Appl. Radiat. Isot. (2000). https://doi.org/10.1016/S0969-8043(00)00114-7
26. K. Debertin, R.G. Helmer, *Gamma- and X-Ray Spectrometry with Semiconductor Detectors* (North Holland, Amsterdam, 1988)
27. Y. Venegas-Argumedo, M.E. Montero-Cabrera, A.I.P. Conf, Proc. (2015). https://doi.org/10.1063/1.4927193
28. M. C. Lépy, T. Altzitzoglou, M. J. Anagnostakis, A. Capogni, A. Ceccatelli, P. De Felice, M. Djurasevic, P. Dryak, A. Fazio, L. Ferreux, A. Giampaoli, J. B. Han, A. Hurtado, A. Kandic, G. Kanisch, K. L. Karfopoulos, S. Klemola, P. Kovar, M. Laubenstein, J. H. Lee, J. M. Lee, K. B. Lee, S. Pierre, G. Carvalhal, O. Sima, Chau Van Tao, Tran Thien Thanh, T. Vidmar, I. Vukanac, M. J. Yang, Appl. Radiat. Isot. (2012). https://doi.org/10.1016/j.apradiso.2012.02.079.
29. M. Asai, A. Dotti, M. Verderi, D.H. Wright, Ann. Nucl. Energy (2015). https://doi.org/10.1016/j.anucene.2014.08.021
30. D. M. Montalván Olivares, M. V. M. Guevara, F. G. Velasco, Appl. Radiat. Isot. (2017). https://doi.org/10.1016/j.apradiso.2017.09.017.
31. P.C. Ortiz-Ramírez, Nucl. Instrum. Methods Phys. Res. A (2015). https://doi.org/10.1016/j.nima.2015.03.05
32. G. Li, Y. Liang, J. Xu, L. Bai, J. Environ. Radioact. (2015). https://doi.org/10.1016/j.jenvrad.2015.04.012
33. G.M. Contessa, S.A. De Crescenzo, P. Rossi, Radioprotection (2021). https://doi.org/10.1051/radiopro/2021019